Ab Initio Calculations for Hydrocarbons: Enthalpy of Formation, Transition State Geometry, and Activation Energy for Radical Reactions

Mark Saeys, Marie-Françoise Reyniers, and Guy B. Marin*

Laboratorium voor Petrochemische Techniek, Universiteit Gent, Krijgslaan 281 S5, B-9000 Gent, Belgium

Veronique Van Speybroeck and Michel Waroquier

Laboratory of Theoretical Physics, Universiteit Gent, Proeftuinstraat 86, B-9000 Gent, Belgium

Received: July 23, 2002; In Final Form: July 10, 2003

A quantum chemical investigation is presented for the determination of accurate kinetic and thermodynamic parameters for hydrocarbon radical reactions. First, standard enthalpies of formation are calculated at different levels of theory for a training set of 58 hydrocarbon molecules, ranging from C_1 to C_{10}, for which experimental data are available. It is found that the CBS-QB3 method succeeds in predicting standard enthalpies of formation with a mean absolute deviation of 2.5 kJ/mol, after a systematic correction of −1.29 kJ/mol per carbon atom and −0.28 kJ/mol per hydrogen atom. Even after a systematic correction, B3LYP density functional theory calculations are not able to reach this accuracy, with mean absolute deviations of 9.2 (B3LYP/6-31G(d)) and 12.9 kJ/mol (B3LYP/6-311G(d,p)), and with increasing deviations for larger hydrocarbons. Second, high-level transition state geometries are determined for 9 carbon-centered radical additions and 6 hydrogen additions to alkenes and alkynes and 10 hydrogen abstraction reactions using the IRCMax(CBS-QB3//B3LYP/6-311G-(d,p)) method. For carbon-centered radical addition reactions, B3LYP/6-311G(d,p) slightly overestimates the length of the forming C−C bond as compared to the IRCMax data. A correlation to improve the agreement is proposed. For hydrogen addition reactions, MPW1K density functional theory (MPW1K/6-31G(d)) is able to locate transition states. However, the lengths of the forming C−H bonds are systematically longer than reference IRCMax data. Here, too, a correlation is proposed to improve the agreement. Transition state geometries for hydrogen abstraction reactions obtained with B3LYP/6-311G(d,p) show good agreement with the IRCMax reference data. Third, the improved transition state geometries are used to calculate activation energies at the CBS-QB3 level. Comparison between both CBS-QB3 and B3LYP density functional theory predictions shows deviations up to 25 kJ/mol. Although main trends are captured by B3LYP DFT, secondary trends due to radical nucleophilic effects are not reproduced accurately.

Introduction

Hydrocarbon radical reactions play an important role in many chemical processes. Atmospheric processes as well as many important industrial processes (e.g., combustion, steam cracking, polymerization, and polymer degradation) proceed via complex radical chemistry involving sometimes hundreds of kinetically significant reaction intermediates.[1−5] Kinetic modeling and mechanistic deductions in any chemical process require accurate kinetic and thermodynamic data. Modeling complex radical reactions thus requires a large number of generally unknown parameters. Estimation of these parameters through the regression of experimental data puts severe limits on the number of kinetic parameters that can be included in the kinetic model. An alternative approach to obtain quantitative values for the kinetic and thermodynamic parameters is therefore desirable.

In this work, we focus on reactions that occur during the steam cracking of hydrocarbons. Steam cracking of oil fractions is the dominant, if not the only, industrial source of light olefins. Steam cracking of hydrocarbons is known to proceed through a free radical mechanism. Three families of reactions can be distinguished: (i) carbon−carbon bond scissions and the reverse radical−radical recombinations; (ii) hydrogen abstraction reactions, both intra- and intermolecular; (iii) β-scissions of radicals and the reverse radical addition to olefins, both intra- and intermolecular.

The first family of reactions generally proceeds on potential energy surfaces that have no clear maximum (i.e., no classical transition state).[6] Within variational transition state theory the activation energy for the carbon−carbon scission reaction is nearly equal to the reaction enthalpy.[6] In contrast, most reactions from the second and third families do have classical transition states.

The increasing capabilities of computational power and the development of better algorithms bring the accurate calculation of kinetic and thermodynamic parameters for industrially relevant reactions from first principles within reach. Free radical reactivity and thermochemistry have been studied with a variety of computational methods, ranging from semiempirical[7,8] over density functional theory[9−19] and post-Hartree−Fock (HF) methods.[20−51] In a series of papers[23,24,26,27,29] Radom and co-workers have assessed the procedures for calculations on radical addition reactions and also on free radical thermochemistry. It is found that calculations on free radicals often require large basis set post-HF methods in order to obtain results with chemical accuracy, that is, better than 2 kcal/mol or 8.4 kJ/

* Author to whom correspondence should be addressed (e-mail Guy.Marin@ugent.be; fax ++32 9 2644999; telephone ++32 9 2644516).

10.1021/jp021706d CCC: $25.00
Published on Web 10/04/2003

mol. On the other hand, computationally less demanding B3LYP density functional theory (DFT)[52,53] is sometimes found to predict accurate kinetic and thermodynamic parameters.[9,10,13,14]

Recently, several theoretical procedures for the reproduction of experimental thermodynamic data with chemical accuracy have been introduced. Three families can be distinguished:

The complete basis set (CBS) methods of Petersson and co-workers[54−57] use a particular basis set extrapolation scheme. These methods are size consistent.[58,59] On the basis of a detailed study, Mayer et al.[26] proposed a modification of the CBS methods, the so-called CBS-RAD methods, for calculations on free radical species. In the original CBS-RAD methods, QCISD/6-31G(d) geometries and frequencies are recommended for radicals with severe spin contamination. This is, however, a very demanding calculation and, if spin contamination[60] is moderate, B3LYP/6-31G(d) may also be recommended.[26]

The Gaussian-*x* methods of Pople and co-workers[61−63] use a different approach to approximate the large basis set post-HF results. These methods achieve accuracy similar to that of the CBS methods for the thermodynamic data from the G2 test set.[64] They are, however, not size consistent, which makes them less appropriate for calculating kinetic parameters. Size consistency is required to obtain continuous potential energy surfaces for bimolecular, such as radical addition and hydrogen abstraction, reactions. Moreover, Mayer et al.[26] find that for radicals with important spin contamination, Gaussian-*x* methods become less reliable.

Martin and de Oliveira[65] have recently proposed the W1 and W2 methods. These methods are developed to achieve calibration accuracy with a mean average deviation of <1 kJ/mol, but they are too computationally demanding for reactions involving more than four symmetrically different first row atoms.

In this paper, we test the CBS-QB3[56,57] and B3LYP[52,53] DFT methods for the calculation of standard enthalpies of formation for a set of hydrocarbons, including alkanes, alkenes, alkynes, and radicals, for which accurate experimental data are available. The size of the molecules ranges from C_1 to C_{10}. Next, we investigate various strategies to locate the transition state for three types of radical reactions: (i) addition of carbon-centered radicals to alkenes and alkynes, (ii) addition of hydrogen radicals to alkenes and alkynes, and (iii) hydrogen abstraction reactions. Finally, activation energies are calculated for a set of radical addition and β-scission reactions and for a set of hydrogen abstraction reactions. A comparative study between CBS-QB3 and B3LYP DFT results is presented.

Computational Methods

Ab initio molecular orbital[58,59] and DFT[66] calculations were performed with the Gaussian98 computational package.[67] Standard enthalpies of formation were computed with the complete basis set CBS-QB3 method[56,57] and with the popular B3LYP[52,53] density functional approach. The complete basis set methods employ the asymptotic convergence of pair natural orbital expansions to extrapolate to the second-order Møller−Plesset (MP2) limit. Higher order contributions to the correlation energy are evaluated with smaller basis sets. The most recent version of the CBS-QB3 method was used in this paper.[57] In this method B3LYP/6-311G(d,p) calculations are performed for geometry optimization and frequency calculation, and MP4(SDQ)/6-31+G(d,p) and CCSD(T)/6-31+G(d′) computations are done to obtain the higher order contributions.

Thermodynamic and kinetic data at the B3LYP/6-311G(d,p) level can be readily obtained from the CBS-QB3 calculations. Because B3LYP calculations are frequently used to study radical thermochemistry and reactivity, we include these results in our discussion. To test the effect of basis set size, B3LYP/6-31G(d) calculations were also performed.

Different types of calculations were performed to locate transition state structures. The highest level transition state geometries were determined using the IRCMax(CBS-QB3//B3LYP/6-311G(d,p))[68] approach. In many high-accuracy theoretical procedures, a mixture of different levels of theory is used. For example, in the CBS-QB3 method, the geometry is optimized with a less expensive computational method (e.g., B3LYP/6-311G(d,p)), whereas the energy for the optimized geometry is obtained from a single-point high-level calculation (extrapolated CCSD(T)/CBS). The IRCMax(CBS-QB3//B3LYP/6-311G(d,p)) approach extends this idea: the intrinsic reaction coordinate (IRC) of the less expensive B3LYP method is searched for the maximum in the high-level CBS-QB3 energy along the less expensive B3LYP reaction path. Malick et al.[68] state that the IRCMax transition state geometry, and in particular the IRC, tends to converge to the optimized high-level geometry, in this case the fully optimized extrapolated CCSD(T)/CBS geometry.

Radical addition reactions were found to have a rather flat potential energy surface around the transition state, which complicates the determination of the transition state. For comparison, the transition states for these reactions were also optimized at the QCISD/6-31G(d) level. The latter method has been recommended by Wong and Radom[24] and by Truhlar and co-workers[48] for transition state geometries.

Transition states for hydrogen atom addition reactions were particularly difficult to locate. For this group of reactions, additional transition state calculations were performed with unrestricted Hartree−Fock (UHF/6-311G(d,p)) and with the new modified Perdew−Wang one-parameter model for kinetics (MPW1K)[69] in combination with different Pople basis sets (6-31G(d), 6-31+G(d), 6-311G(d,p)),[58] in order to find an inexpensive computational procedure that can yield transition state structures in agreement with the high-level IRCMax reference data.

Activation energies were computed with CBS-QB3 and also with B3LYP/6-311G(d,p) and B3LYP/6-31G(d) for a comparative analysis. Rate coefficients can be obtained with eq 1,[70] in

$$k = \kappa(T)\,\frac{k_B T}{h}\,\frac{Q_{TS}(T)}{Q_{react}(T)}\exp\left(\frac{-\Delta E(0\text{ K})}{RT}\right) \qquad (1)$$

which $\kappa(T)$ is the tunneling correction, k_B is the Boltzman constant, and h is the Planck constant. $Q_x(T)$ stands for the partition functions evaluated at temperature T, and $\Delta E(0\text{ K})$ is the energy difference between the reactants and the transition state, including the zero-point energy difference. For the computation of accurate partition functions particular attention to internal rotations is required.[29,42,71,72] In this paper, we focus on the activation energy at 0 K, $\Delta E(0\text{ K})$.

Results and Discussion

This section is divided into three parts. In the first part, standard enthalpies of formation for a test set of hydrocarbons are calculated and compared to experimental values. In the second part, transition state geometries are discussed for three types of reactions: carbon-centered radical addition, hydrogen radical addition and hydrogen abstraction reactions. In the third section, activation energies are determined and their behavior is discussed.

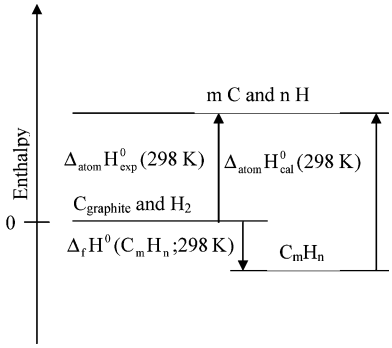

Figure 1. Illustration of the calculation of standard enthalpies of formation from ab initio standard enthalpies of atomization.

Standard Enthalpy of Formation for Stable Molecules. Standard enthalpies of formation were calculated for 64 hydrocarbon molecules -alkanes, alkenes, alkynes and radicals- that are involved in the steam cracking of hydrocarbons and for which experimental data are available. The CBS-QB3, B3LYP/6-311G(d,p) and B3LYP/6-31G(d) methods were applied. Standard enthalpies of formation are calculated with eq 2.

$$\Delta_fH°(C_mH_n;\ 298\ K) = m\Delta_fH°_{exptl}(C;\ 298\ K) + n\Delta_fH°_{exptl}(H;\ 298\ K) - [mH°_{calcd}(C;\ 298\ K) + nH°_{calcd}(H;\ 298\ K) - H°_{calcd}(C_mH_n;\ 298\ K)] \quad (2)$$

$$C_mH_n \rightarrow mC + nH \quad (3)$$

The last three terms of eq 2 yield the calculated atomization enthalpy for C_mH_n, that is, the reaction enthalpy of eq 3. Equation 2 is visualized in Figure 1. It can be seen that $\Delta_fH°(C_mH_n;\ 298\ K)$ is obtained by subtracting the calculated atomization energy for C_mH_n from the experimental $\Delta_fH°$ (298 K) for the constituting atoms. Table 1 lists the experimental values for the standard enthalpies of formation for the test set of hydrocarbons and the deviations with the theoretical predictions from the computational methods under consideration. Most experimental values were obtained from a recent compilation by Cioslowski et al.[73] and from the NIST Chemistry WebBook.[74] For some molecules, two or more significantly different experimental values were found in the literature. Of these, one experimental value was selected for comparison with the ab initio predictions and set in boldface in Table 1. The choice was based on the compilation by Cioslowski et al.[73] or on the value in the G3/99 test set.[75] For the ethynyl radical, the experimental value of Tsang[76] was preferred over the JANAF value,[77] because the experimental error on the standard enthalpy of formation was reported in the former study. For 2,3-dimethyl-2-butene, the most recent experimental value was selected. The deviations of the theoretical predictions are given in columns 4, 6, and 8 of Table 1. For both B3LYP methods a systematic increase of the deviation with the number of carbon atoms is noticed. This systematic increase of the deviations is not so obvious for the CBS-QB3 method. The statistics of the deviations over the complete test set are summarized in Table 2 for the different levels of theory. The CBS-QB3 method overestimates the experimental enthalpies of formation with an average deviation of 8.89 kJ/mol. With a mean absolute deviation (MAD) of 9.04 kJ/mol, this method does not achieve the required chemical accuracy over the test set. The maximum deviation of +26.3 kJ/mol was found for *o*-benzyne, but the experimental error for this molecule amounts to 13.8 kJ/mol. For the B3LYP/6-31G(d) and the B3LYP/6-311G(d,p) methods a serious overestimation of the experimental enthalpies is observed. We find average deviations of +30.92 and +49.76 kJ/mol, respectively, MADs of 31.11 and 50.09 kJ/mol, and maximal deviations of +89.77 and +142.34 kJ/mol for 2,2,3,3-tetramethylbutane, for which the standard enthalpy of formation is accurately known experimentally. These deviations are too large to recommend the B3LYP method as a suitable tool for the accurate prediction of standard enthalpies of formation of hydrocarbon molecules. It is remarkable that the B3LYP/6-31G(d) method performs significantly better than the B3LYP/6-311G(d,p) method. In general, B3LYP DFT underestimates the bond energies, yielding atomization energies that are too low and enthalpies of formation that are too high. Using a smaller basis set increases the basis set superposition error (BSSE),[80] which artificially stabilizes the molecule and increases the calculated bond energies. The MAD between the values of the two B3LYP DFT methods amounts to 19.86 kJ/mol over the test set, and the deviations between the predicted standard enthalpies of formation increase with the size of the hydrocarbon.

The accurate calculation of atomization enthalpies is one of the most challenging tasks for quantum chemistry (e.g., Koch and Holthausen[66]). Especially in DFT with currently available functionals, the calculation of atomic energies is known to be problematic.[66,81] Moreover, in the calculation of standard enthalpies of formation with eq 2, deviations on the computed atomic energies are multiplied by the number of atoms in the molecule. The small but non-negligible experimental error on the standard enthalpy of formation of the carbon atom, that is, 0.5 kJ/mol, is multiplied with the number of carbon atoms as well.

In panels a and c of Figure 2, the deviations of the B3LYP standard enthalpies of formation with the experimental values are plotted versus the number of carbon atoms in the molecule. As already noted, the deviations increase with the size of the molecule. The increase is less pronounced for the small basis set method. A similar, although less explicit, increase is found with the number of hydrogen atoms in the molecule. This behavior of the B3LYP method has been reported in other work as well.[75,82] Note that also for the CBS-QB3 method a small and systematic increase of the experimental deviations with the size of the molecule can be observed (Figure 2e).

To remove these systematic deviations, we replaced the experimental standard enthalpy of formation of the carbon atom in eq 2 by *X* and that of the hydrogen atom by *Y*:

$$\Delta_fH°(C_mH_n;\ 298\ K) = mX + nY - \Delta_{atom}H°(C_mH_n;\ 298\ K) \quad (4)$$

The parameters *X* and *Y* were determined by a linear regression of eq 4 against the experimental enthalpies of formation. This fitting procedure should not be interpreted as if the experimental enthalpies of formation of the carbon and the hydrogen atom were estimated, but rather as the elimination of systematic deviations that occur per hydrogen and per carbon atom. Only enthalpies of formation with an experimental error of <3.1 kJ/mol were used in the regression procedure, that is, 58 values.

A value of 710.05 kJ/mol was detemined for *X* for the B3LYP/6-31G(d) calculations, and 707.35 kJ/mol was determined for *X* for the B3LYP/6-311G(d,p) calculations. These values should be compared with the experimental standard enthalpy of formation of the carbon atom, that is, 716.7 (0.5) kJ/mol.[74] For *Y*, values of 217.83 kJ/mol (B3LYP/6-31G(d)) and 216.62 kJ/mol (B3LYP/6-311G(d,p)) were found, which

TABLE 1: Deviations between ab Initio and Experimental Standard Enthalpies of Formation for Various Computational Methods (kJ/mol)

			deviation (theory-exptl)					
molecule	ΔH_f °(exptl)	source[a]	CBS-QB3	CBS-QB3*	B3LYP/ 6-31G(d)	B3LYP*/ 6-31G(d)	B3LYP/ 6-311G(d,p)	B3LYP*/ 6-311G(d,p)
H	218.0	NIST	0	−0.3	0	−0.2	0	−1.4
H_2	0.0	NIST	−4.7	−5.3	−0.4	−0.7	−1.4	−4.2
C	716.7 (0.5)	NIST	0	−1.3	0	−6.6	0	−9.3
CH_3 (methyl radical)	**146.6** (0.4)	CIOSL	2.3	0.2	−1.3	−8.5	−2.4	−15.9
	145.7 (NN)	NIST						
CH_4 (methane)	−74.9 (0.4)	CIOSL	0.8	−1.6	−0.4	−7.7	2.8	−12.0
C_2H (ethynyl radical)	**556.0** (8.0)	NIST	17.5	14.6	42.4	29.0	34.2	14.1
	477.0 (NN)	NIST						
C_2H_2 (ethyne)	**226.9** (0.8)	NIST	7.6	4.6	33.5	19.9	22.2	0.8
	228.3 (NN)	PED						
C_2H_3 (vinyl radical)	299.7 (3.3)	CIOSL	1.0	−2.3	5.3	−8.4	2.3	−20.5
C_2H_4 (ethene)	52.3 (0.4)	CIOSL	3.7	0.0	14.2	0.3	14.2	−10.0
C_2H_5 (ethyl radical)	**120.9** (1.7)	CIOSL	4.7	0.7	−2.3	−16.3	4.1	−21.5
	119.0 (2.0)	NIST						
C_2H_6 (ethane)	**−83.7** (0.4)	CIOSL	1.8	−2.4	1.5	−12.8	12.0	−14.9
	−84.7 (0.5)	NIST						
C_3H_3 (propargyl radical)	339.0 (4.0)	NIST	17.7	13.1	24.1	3.8	20.3	−11.8
C_3H_4 (propyne)	**184.9** (0.8)	CIOSL	7.1	2.2	29.9	9.4	27.0	−6.5
	185.4 (0.9)	NIST						
C_3H_4 (allene)	190.4 (1.3)	CIOSL	4.9	0.0	11.6	−8.9	13.1	−20.4
C_3H_5 (allyl radical)	171.0 (3.0)	NIST	1.6	−3.6	2.7	−18.0	8.6	−26.3
C_3H_6 (propene)	20.1 (0.8)	CIOSL	5.6	0.1	16.3	−4.6	24.7	−11.6
C_3H_7 (1-propyl radical)	100.0 (2.0)	NIST	7.7	1.9	7.7	−13.3	19.4	−18.3
C_3H_7 (2-propyl radical)	90.0 (2.0)	NIST	5.0	−0.8	−1.2	−22.3	12.6	−25.0
C_3H_8 (propane)	−104.7 (0.4)	CIOSL	3.8	−2.3	8.9	−12.3	26.5	−12.6
C_4H_4 (3-buten-1-yne)	296.2 (2.1)	CIOSL	2.9	−3.3	29.7	2.6	27.4	−15.4
C_4H_6 (1,3-butadiene)	**110.1** (0.8)	CIOSL	9.7	3.0	26.8	−0.7	34.9	−10.7
	111.9 (1.0)	NIST						
	108.8 (0.8)	NIST						
C_4H_6 (1,2-butadiene)	**162.4** (0.4)	CIOSL	7.2	0.4	15.7	−11.8	25.5	−20.1
	165.4 (1.2)	NIST						
C_4H_6 (1-butyne)	165.2 (0.9)	NIST	10.0	3.3	37.6	10.1	41.8	−3.8
C_4H_8 (1-butene)	0.0 (0.8)	CIOSL	7.6	0.3	24.3	−3.5	39.7	−8.7
C_4H_8 (isobutene)	**−16.7** (0.8)	CIOSL	7.2	−0.1	23.4	−4.4	40.6	−7.7
	−17.9 (1.1)	NIST						
C_4H_9 (2-butyl radical)	69.0 (2.0)	NIST	7.4	−0.2	7.4	−20.6	28.2	−21.5
C_4H_9 (1-isobutyl radical)	70.0 (2.0)	NIST	11.5	4.0	20.8	−7.1	40.7	−9.0
C_4H_9 (ter-isobutyl radical)	**51.5** (1.7)	CIOSL	8.6	1.0	7.1	−20.9	29.2	−20.5
	48.0 (3.0)	NIST						
C_4H_{10} (isobutane)	**−134.4** (0.8)	CIOSL	5.9	−2.0	21.9	−6.2	46.2	−4.9
	−135.6 (0.5)	NIST						
C_5H_6 (3-methyl-3-buten-1-yne)	259 (NN)	NIST	6.0	−2.0	44.0	9.9	45.2	−9.7
C_5H_8 (3-methyl-1-butyne)	136.4 (2.1)	NIST	13.2	4.6	50.9	16.5	62.4	4.7
C_5H_8 (1,3-pentadiene)	76.2 (0.8)	CIOSL	12.4	3.9	30.3	−4.1	47.2	−10.5
C_5H_8 (1,4-pentadiene)	106.3 (1.3)	NIST	10.0	1.5	40.8	6.4	51.7	−5.9
C_5H_8 (2-methyl-1,3-butadiene)	75.7 (1.0)	NIST	10.5	1.9	47.8	13.4	53.0	−4.7
C_5H_8 (3-methyl-1,2-butadiene)	129.1 (0.6)	NIST	8.4	−0.1	23.1	−11.3	41.5	−16.2
C_5H_8 (cyclopentene)	**33.9** (1.3)	CIOSL	11.3	2.7	38.9	4.5	63.7	6.1
	36.0 (NN)	NIST						
C_5H_{10} (3-methyl-1-butene)	−27.4 (0.9)	NIST	8.0	−1.1	38.8	4.0	58.0	−2.4
C_5H_{10} (2-methyl-2-butene)	−41.5 (0.9)	NIST	9.1	0.0	28.2	−6.5	54.5	−5.9
C_5H_{10} (cyclopentane)	−76.4 (0.8)	NIST	9.7	0.6	35.3	0.6	67.4	7.0
C_5H_{11} (2-methyl-2-butyl radical)	28.0 (3.0)	NIST	15.1	5.7	21.6	−13.3	51.0	−10.8
C_5H_{11} (neopentyl radical)	37.3 (4.0)	COHEN	14.1	4.7	39.9	4.9	65.9	4.1
C_5H_{12} (neopentane)	−168.7 (1.3)	CIOSL	8.1	−1.6	39.6	4.5	71.6	8.4
C_6H_4 (*o*-benzyne)	**443.3** (13.8)	CIOSL	26.3	17.6	71.1	30.8	86.6	25.2
	490.0 (20.0)	NIST						
C_6H_5 (phenyl radical)	339.9 (2.5)	NIST	13.3	4.3	21.6	−18.9	45.1	−17.7
C_6H_6 (benzene)	82.5 (0.8)	CIOSL	8.5	−0.8	34.1	−6.6	57.9	−6.3
C_6H_8 (1,3-cyclohexadiene)	**106.3** (0.8)	G3	13.9	4.1	48.3	7.2	74.4	7.4
	104.6 (0.6)	NIST						
C_6H_8 (1,4-cyclohexadiene)	**104.7** (0.4)	G3	16.1	6.3	50.5	9.5	76.5	9.5
	100.4 (3.1)	NIST						
	109.0 (NN)	NIST						
C_6H_{10} (cyclohexene)	−4.3 (1.0)	NIST	11.6	1.2	45.9	4.5	79.3	9.6
C_6H_{10} (3,3-dimethyl-1-butyn)	107.0 (1.3)	NIST	10.8	0.5	64.7	23.3	83.3	13.5
C_6H_{12} (cyclohexane)	−123.5 (0.8)	CIOSL	10.5	−0.4	44.8	3.1	85.8	13.3
C_6H_{12} (2,3-dimethyl-2-butene)	**70.3** (1.5)	NIST	16.6	5.6	44.8	3.1	80.1	7.6
	−68.4 (1.5)	NIST						

TABLE 1 (Continued)

molecule	$\Delta H_f°$(exptl)	source[a]	deviation (theory-exptl) CBS-QB3	CBS-QB3*	B3LYP/ 6-31G(d)	B3LYP*/ 6-31G(d)	B3LYP/ 6-311G(d,p)	B3LYP*/ 6-311G(d,p)
C_6H_{12} (3,3-dimethyl-1-butene)	−59.8 (1.5)	NIST	9.8	−1.1	56.0	14.3	85.4	12.9
C_6H_{14} (2,3-dimethylbutane)	−177.8 (1.0)	NIST	9.8	−1.7	48.3	6.2	87.2	11.9
C_7H_7 (benzyl radical)	207.0 (4.0)	NIST	13.8	3.0	32.5	−14.9	63.0	−11.9
C_7H_8 (toluene)	50.2 (0.4)	CIOSL	9.5	−1.6	40.6	−7.1	73.9	−2.4
C_7H_{14} (methylcyclohexane)	−154.8 (1.0)	NIST	11.6	−1.1	57.7	9.0	106.0	21.4
C_8H_8 (styrene)	**147.8** (1.7)	CIOSL	11.7	−0.6	51.2	−3.0	85.1	−0.6
	146.9 (1.0)	NIST						
C_8H_{10} (ethylbenzene)	29.8 (0.8)	NIST	9.6	−3.3	48.8	−5.8	89.3	0.9
C_8H_{18} (2,2,3,3-tetramethylbutane)	−225.9 (1.9)	NIST	9.3	−5.8	89.8	33.8	142.3	42.9
C_9H_{10} (α-methylstyrene)	118.3 (1.4)	NIST	10.4	−3.8	60.8	−0.4	103.5	5.8
C_9H_{12} (cumene)	3.9 (1.1)	NIST	10.1	−4.7	62.4	0.9	110.3	9.8
$C_{10}H_{14}$ (*tert*-butylbenzene)	3.9 (1.1)	NIST	10.5	−6.0	56.8	−11.7	138.6	26.0

[a] NIST, ref 74; CIOSL = ref 73; G3 = ref 75; COHEN = ref 78; PED = ref 79.

TABLE 2: Summary of the Deviations for ab Initio Standard Enthalpies of Formation for Various Computational Methods (Theory−Exptl) (kJ/mol)

method	av	MAD	RMS	max
CBS-QB3	8.89	9.04	10.21	26.30
CBS-QB3*	0.19	2.48	2.89	6.25
B3LYP/6-31G(d)	30.92	31.11	37.35	89.77
B3LYP/6-31G(d)*	−1.40	9.17	11.50	33.84
B3LYP/6-311G(d,p)	49.76	50.09	60.07	142.34
B3LYP/6-311G(d,p)*	−3.82	12.94	13.79	42.90

should be compared with 218.0 kJ/mol.[74] The deviation of *X* and *Y* from the experimental values indicates that an important systematic error in B3LYP calculations takes place, in particular for the carbon atom. Also, the systematic corrections are smaller for B3LYP/6-31G(d) than for B3LYP/6-311G(d,p). Removing the systematic errors significantly improves the calculated enthalpies of formation. The combination of the B3LYP results with the systematic corrections is indicated by B3LYP*. The latter results are listed in colums 7 and 9 of Table 1. The statistics of the deviations are reported in Table 2. The systematic corrections reduce the MAD over the test set almost 4-fold, from 31.11 to 9.17 kJ/mol for B3LYP/6-31G(d) and from 50.09 to 12.94 kJ/mol for B3LYP/6-311G(d,p). However, maximum deviations of +33.8 and +42.9 kJ/mol are still observed for 2,2,3,3-tetramethylbutane. In Figure 2b,d the deviations of the B3LYP* values with the experimental data are plotted versus the number of carbon atoms. All data were plotted, also those for which the experimental error is large. These plots indicate that still large deviations are to be expected for the larger hydrocarbon molecules, in particular, for the B3LYP*/6-311G(d,p) method.

Applying a similar approach for the CBS-QB3 method leads to an *X* value of 715.41 kJ/mol and a *Y* value of 217.72 kJ/mol. The difference with the experimental atomic enthalpies of formation is small, resulting in systematic corrections of only −1.29 kJ/mol per carbon atom and −0.28 kJ/mol per hydrogen atom. Part of the corrections can be attributed to core−valence correlation and also to scalar relativistic effects, which are both neglected in CBS-QB3. Scalar relativistic effects are known to reduce atomization energies in most cases,[49,83] whereas core−valence correlation often increases the calculated atomization energies.[49,83] The resulting standard enthalpies of formation are reported in Table 1 under CBS-QB3*. The statistics of the deviations for this method give an average deviation of 0.19 kJ/mol and a MAD of only 2.48 kJ/mol, which is again almost 4 times better than without the systematic corrections, despite the small value of the corrections. Figure 2f shows an overview of the deviations with the experimental values versus the carbon number. The solid lines in Figure 2f indicate the rms error of the CBS-QB3* method, which is a measure for the standard deviation of the method. Large deviations are found for the ethynyl radical (+14.6 kJ/mol), for the propargyl radical (+13.1 kJ/mol), and for *o*-benzyne (+17.6 kJ/mol). However, the experimental enthalpies of formation of these molecules have large error bars, and a re-examination of the experimental values seems to be warranted. Significant deviations are also observed for the alkynes: ethyne (+4.6 kJ/mol), propyne (+2.2 kJ/mol), 1-butyne (+3.3 kJ/mol), and 3-methyl-1-butyne (+4.6 kJ/mol). Part of the deviation could be related to the underestimation of the triple C−C bond length by the B3LYP method (119.8 vs 120.3 pm[66]), which is used for the geometry optimization in CBS-QB3. Recently, Feller and Dixon[50] performed very detailed quantum chemical calculations including relativistic and core−valence correlation effects for a set of model hydrocarbons. The largest deviation with experiment was found for ethyne. Their calculated value of 229.8 kJ/mol is in better agreement with our CBS-QB3* value. On the other hand, on the basis of W2 theory, Parthiban et al.[51] reported an enthalpy of formation of 228.1 kJ/mol, which is closer to the reported experimental value.

Important deviations are also observed for some radical species, but these deviations should be compared with the substantial error bars on the experimental enthalpies, and the deviations are therefore not very significant. The calculated enthalpies of formation of 1,3-cyclohexadiene (110.4 kJ/mol) and 1,4-cyclohexadiene (111.0 kJ/mol) are higher than the selected experimental values. The experimental value for 1,4-cyclohexadiene reported by Roth et al.,[84] 109.0 kJ/mol, is however in better agreement with our ab initio value. These authors did not determine a value for 1,3-cyclohexadiene. However, on the basis of the experimental enthalpy difference between 1,3- and 1,4-cyclohexadiene, an enthalpy closer to the ab initio value can also be expected for 1,3-cyclohexadiene. One of the largest deviations in the test set was found for dihydrogen (−5.3 kJ/mol). In this molecule the hydrogen atom is not bonded to a carbon atom. Dihydrogen therefore has a different bonding pattern and, in principle, does not belong in the hydrocarbon test set. Also, the systematic correction for the hydrogen atom can be partly related to a bond additivity correction for the C−H bond. For this reason the calculated standard enthalpy of formation of dihydrogen does not improve after the systematic correction.

All previous approaches use the theoretical atomization energies as the central quantity. An alternative would be to replace the atomization reaction (eq 3) by, for example, the following reaction:

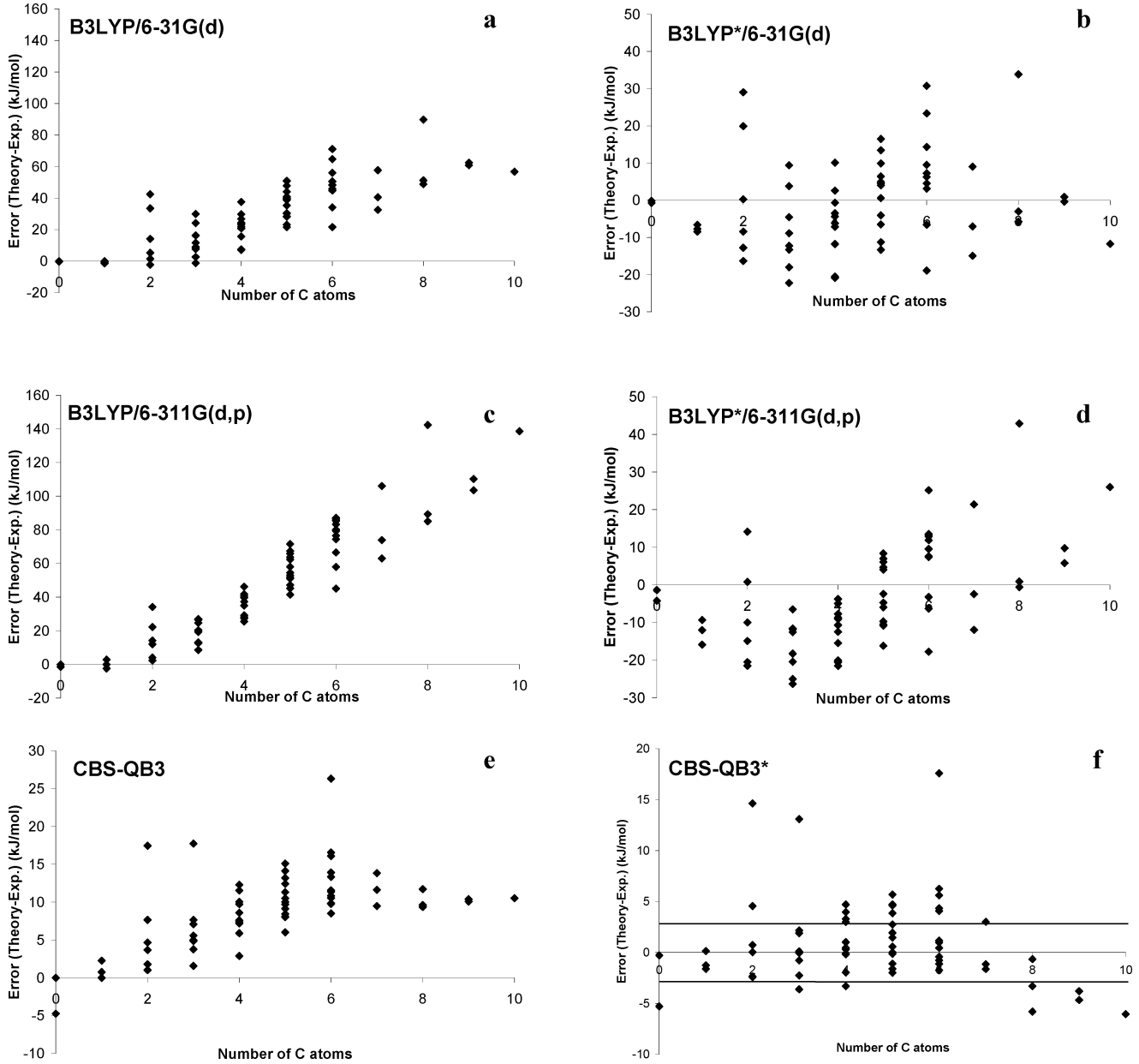

Figure 2. Deviations of different computational methods from experimental standard enthalpies of formation (kJ/mol) as a function of the number of carbon atoms. * indicates methods applying the systematic corrections as described in the text. The horizontal solid lines in (f) indicate the rms error of the CBS-QB3* method.

$$C_mH_n \rightarrow mCH_4 + {}^1/_2(n - 4m)H_2 \qquad (5)$$

This changes the top level in Figure 1 and thus will yield different calculated enthalpies of formation. For the CBS-QB3 method, this new approach increases the MAD significantly, from 9.04 to 20.00 kJ/mol. This is due to the deviation of the calculated enthalpy of formation for dihydrogen with the CBS-QB3 method. For the B3LYP/6-311G(d,p) method, however, the MAD decreases from 50.08 to 31.33 kJ/mol. With the new approach, atomic calculations are circumvented, which causes a significant improvement. This is probably related to the problems of atomic DFT calculations with currently available functionals.[66,81] Caution is however required, because for the B3LYP/6-31G(d) method, the MAD is nearly unaffected, decreasing from 31.11 to 31.01 kJ/mol.

More alternative reactions could be envisaged, thereby changing the top level in Figure 1. However, the standard enthalpies of formation that can be obtained by using different reactions of this type cannot be better than the values obtained by regression of the experimental data using eq 4. Indeed, in the latter case the position of the top level in Figure l is optimized to yield the smallest possible deviations.

From this paragraph it can be concluded that the CBS-QB3* method can be regarded as a reliable tool to compute accurate standard enthalpies of formation for hydrocarbon molecules with a MAD of 2.48 kJ/mol. Similar MADs have been reported in assessment calculations for the Gaussian-*x* methods over a smaller test set of the 38 hydrocarbon molecules from the G3/99-test set.[75] For G3, the reported MAD amounts to 2.89 kJ/mol,[75] for G3S it amounts to 3.31 kJ/mol,[85] and for G3X, 2.34 kJ/mol.[63]

The MAD of 9.17 kJ/mol reported in this study for the B3LYP*/6-31G(d) method is far better than the MAD of 24.06 kJ/mol reported for the B3LYP/6-311+G(3df,2p) method for the 38 hydrocarbon molecules of the G3/99 test set.[75] The increase of the deviations with the size of the molecule, even after a systematic correction, limits the reliability of B3LYP

TABLE 3: Transition State Geometries for Carbon-Centered Radical Addition Reactions from Various Computational Methods and Potential Energy Barriers at the CBS-QB3 Level for Corresponding Geometries

	IRCMax		B3LYP/6-311G(d,p)		QCISD/6-31G(d)
reaction	distance[a]	E_a	distance[a]	E_a	distance[a]
$CH_2{=}CHCH_2^{\bullet} + CH_2{=}CH_2$	213.3	45.90	214.3	45.86	214.2
$CH{\equiv}CCH_2^{\bullet} + CH_2{=}CH_2$	216.9	34.57	217.8	34.54	217.4
$CH_3^{\bullet} + CH_2{=}CH_2$	229.2	21.57	233.2	21.12	227.2
$CH_3CH_2^{\bullet} + CH_2{=}CH_2$	227.7	18.66	230.1	18.51	226.5[b]
$(CH_3)_2CH^{\bullet} + CH_2{=}CH_2$	226.8	13.82	227.6	13.80	225.1
$CH_2{=}CH^{\bullet} + CH_2{=}CH_2$	235.7	8.62	238.7	8.46	229.9[b]
$CH_3^{\bullet} + CH_3\mathit{C}H{=}CH_2$[c]	228.0	26.30	230.5	26.09	not calcd
$CH_3^{\bullet} + CH{\equiv}CH$	226.8	29.82	230.3	29.42	224.8
$CH_3^{\bullet} + \mathit{C}H_2{=}CHCH{=}CH_2$[c]	239.6	9.23	246.5	8.45	238.0

[a] Length (pm) of the forming C−C bond between the radical and the alkene. [b] TS with Cs symmetry. [c] Methyl radical attacks the carbon atom printed in italics.

DFT for larger molecules. Indeed, a MAD of 9.17 kJ/mol and a maximum deviation of +33.84 kJ/mol are too large to apply B3LYP* with confidence to calculate accurate standard enthalpies of formation for hydrocarbons.

Transition State Geometry. Calculations on transition states of radical reactions are particularly difficult.[48] The sources of the difficulties are the increase of dynamical electron correlation in proceeding from the reactants to the transition state and the problem of spin contamination of the unrestricted HF wave function, in particular at the transition state. Chuang et al.[48] conclude that UQCISD and UCCSD with sufficiently flexible basis sets are required to predict accurate transition state geometries. Unfortunately, such optimizations and frequency calculations are too demanding to use routinely for the radical reactions we want to study.

In the CBS-QB3 approach B3LYP/6-311G(d,p) geometries and frequencies are used. It is therefore important to assess the accuracy of this method for locating the transition state along the reaction path. From the literature, it is found that B3LYP DFT tends to overestimate the lengths of the weak C−C and C−H bonds in the transition state of radical addition reactions.[29,66,69] Because no experimental data on transition state geometries exist, B3LYP can only be benchmarked against results from high-level calculations.

Recently, Malick et al.[68] introduced the IRCMax method. In this section we use this approach to locate high-level transition states for three types of reactions: (i) the addition of carbon-centered radicals to alkenes and alkynes, (ii) the addition of hydrogen atoms to alkenes and alkynes, and (iii) the abstraction of hydrogen atoms by radicals. In our approach, single-point CBS-QB3 energies were calculated at different points along the B3LYP/6-311G(d,p) intrinsic reaction path in steps of 5 pm $amu^{-1/2}$. Steps were taken until three consecutive points were found of which the middle one is higher in CBS-QB3 energy than the other two. Then a parabola was fit through those three points to locate the transition state. In the following, we will abbreviate this procedure as IRCMax. Characteristic bond lengths of this reference transition state geometry were compared with values from other theoretical methods.

Carbon-Centered Radical Addition to Alkenes. The addition of carbon-centered radicals to alkenes and to substituted alkenes has received considerable attention. Fischer and Radom recently reviewed the experimental and theoretical literature and discussed the factors controlling the rates of these reactions.[30] In this paper we studied nine reactions, four in which a methyl radical adds to different alkenes and five in which different types of radicals add to ethene. The reactions were chosen to cover a wide range of activation energies and transition state C−C bond lengths. Table 3 lists the calculated transition state bond lengths

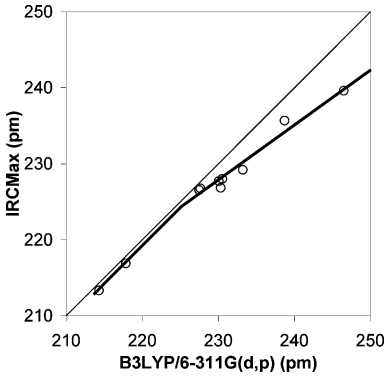

Figure 3. Bond lengths (pm) of the forming C−C bond in the transition state of the carbon-centered radical addition to alkenes: IRCMax(CBS-QB3//B3LYP/6-311G(d,p)) values versus B3LYP/6-311G(d,p) values (Table 3).

for the forming C−C bond. Bond lengths were calculated with both the IRCMax and B3LYP methods. Table 3 also gives the CBS-QB3 potential energy barriers for both the IRCMax and B3LYP geometries. For comparison, some expensive QCISD/6-31G(d) optimized bond lengths are reported as well. As discussed, this method has been recommended for geometry optimizations for radical reactions.[24,48] At first sight, the optimized C−C distances from the B3LYP calculation are close to the IRCMax reference values. This results in very similar potential energy barriers, with the IRCMax values of course being slightly higher. A closer look, however, reveals that B3LYP always overestimates the length of the forming C−C bond as compared to the IRCMax value and that for the longer bonds the overestimation is largest, specifically, methyl radical addition to butadiene. Although the difference in potential energy barrier is small, for reactions with an early transition state, that is, a long forming C−C bond, and a low potential energy barrier, the difference can amount to 1 kJ/mol, which is a deviation of 10% of the barrier. The C−C bond lengths from the QCISD/6-31G(d) method are always within 2 pm of the IRCMax values.

In Figure 3 the B3LYP-optimized C−C distance is plotted versus the corresponding IRCMax value. The overestimation by B3LYP is fairly systematic, and the agreement can be improved by a linear correlation. For B3LYP C−C bond lengths longer than 225 pm the correlation between the IRCMax and B3LYP/6-311G(d,p) bond lengths can be expressed as

$$C{-}C_{IRCMax} = 0.7381C{-}C_{B3LYP} + 58.03\ \text{pm} \qquad (6)$$

For shorter distances, the difference between the B3LYP/6-311G(d,p) and IRCMax lengths becomes very small. For the

TABLE 4: Transition State Geometries for Hydrogen Radical Addition Reactions from Various ab Initio Methods and Potential Energy Barriers at the CBS-QB3 Level for the IRCMax and B3LYP/6-311G(d,p) Geometries

	IRCMax		B3LYP/6-311G(d,p)		UHF	QCISD	MPW1K
reaction	distance[a]	E_a	distance[a]	E_a	distance[a]	distance[a]	distance[a]
$H^\bullet + CH_2{=}CH_2$	200.2	5.87	223.7	3.53	198.3	190.3	215.3
$H^\bullet + CH{\equiv}CH$	190.9	14.02	202.1	12.74	188.3	184.5	197.9
$H^\bullet + CH_3\mathit{C}H{=}CH_2$[b]	192.3	9.70	203.1	8.43	194.1	186.9	201.6
$H^\bullet + \mathit{C}H_2{=}CHCH{=}CH_2$[b]	211.9	−0.93[c]	no TS		221.8	202.7	239.1
$H^\bullet + CH_2{=}\mathit{C}{=}CH_2$[b]	191.3	14.41	197.6	13.72	199.5	187.6	195.4
$H^\bullet + \mathit{C}H_2{=}C(CH_3)_2$[b]	204.0	1.01	no TS		198.0	192.2	224.9

[a] Length (pm) of the forming C−H bond between the hydrogen atom and the alkene. [b] Hydrogen attacks the carbon atom printed in italics. [c] See text.

propargyl and allyl radical addition to ethene, bond lengths are larger by 0.97 and 0.94 pm. We propose to use a shift of −0.957 pm for bond lengths shorter than 225 pm. The corresponding correlation is shown in Figure 3 by the solid line.

Next, we reoptimized the transition state geometry at the B3LYP/6-311G(d,p) level of the CBS-QB3 method, keeping the forming C−C bond length constrained at the value obtained from eq 6. The other (nonconstrained) internal coordinates of the reoptimized transition state geometries were compared with geometries obtained at the QCISD/6-31G(d) level. It is found that the nonconstrained internal coordinates are in better agreement with the high-level QCISD values when the C−C bond is contrained at the value obtained from eq 6 than the values obtained for the fully optimized B3LYP/6-311G(d,p) transition state.

Hydrogen Radical Addition to Alkenes. The addition of hydrogen atoms to ethene has been studied theoretically by different groups.[12,22,29,30] It is found that DFT approaches have considerable problems in finding and optimizing the transition state structure for this reaction. In general, DFT overestimates the forming C−H bond length and underestimates the potential energy barrier for the hydrogen radical addition reaction; that is, DFT locates the transition state for the addition reaction too early.

Here, we studied the reaction path on the potential energy surface for six hydrogen atom addition reactions. The reactions were selected to cover a wide range in transition state C−H bond lengths and activation energies. The optimized transition state C−H bond lengths for the B3LYP/6-311G(d,p) and the IRCMax method as well as the corresponding CBS-QB3 potential energy barrier are listed in Table 4. The barriers for hydrogen addition reactions are quite low, ∼15 kJ/mol lower than barriers for similar methyl radical addition reactions. For the addition of H to butadiene, forming a secondary allylic radical, the calculated energy of the transition state lies lower in energy than the separated reactants, leading to a negative potential energy barrier. Calculation of the CBS-QB3 energy for several points along the reaction path near the transition state confirmed that the obtained geometry is indeed a transition state. The energies for those points are all lower than the energy of the transition state's geometry. The negative barrier is caused by a discontinuity in the CBS-QB3 energy along the reaction path at a C−H distance of ∼225 pm. Along the reaction path, there is a sudden switch from the reactant configuration to the product configuration. As a result, the UHF energy shows a discontinuity of about −30 kJ/mol at this point. At the CCSD(T) level, the discontinuity in the energy is reduced to +4 kJ/mol. Also, the spin contamination of the wave function changes discontinuously: $\Delta(S^2)$ changes from 0.11 at the reactant side to 0.45 at the product side for a difference in C−H distance of 2 pm. Because the CBS-QB3 method includes a spin contamination correction, this leads to a discontinuity in the CBS-QB3 energy of −8.5 kJ/mol. Together with the CCSD(T) gap, this leads to a discontinuity of −4.5 kJ/mol in the CBS-QB3 energy. As a consequence, the CBS-QB3 energy suddenly drops by ∼4 kJ/mol at a C−H bond length of 225 pm, that is, before the transition state, causing the negative value for the potential energy barrier in this study. For a correct description of the reaction path, multireference (MR) methods would be required. However, MR equivalents of the CBS-QB3 method are still under development,[86] and MRCI calculations for molecules of the size we want to study are too demanding. Fortunately, the CCSD(T) method removes most of this discontinuity, reducing it to <4 kJ/mol.

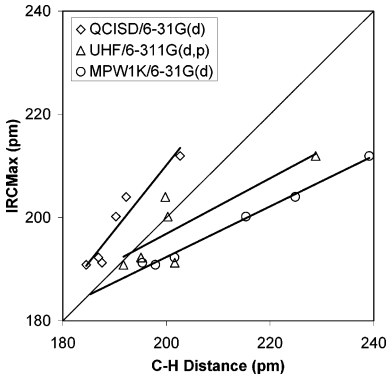

Figure 4. Bond lengths (pm) of the forming C−H bond in the transition state of the hydrogen radical addition to alkenes: values from various levels of theory versus IRCMax(CBS-QB3//B3LYP/6-31G(d,p)) values.

All B3LYP calculations show a significant overestimation of the forming C−H distance at the transition state as compared to the IRCMax reference value. This leads to an underestimation of the activation energy. For two reactions, that is, hydrogen addition to isobutene forming the ter-isobutyl radical and to butadiene forming the 1-buten-3-yl radical, no transition state could be located. These reactions have a very flat potential energy surface going from the reactant to the transition state and, therefore, require a very accurate description of the potential energy. Because B3LYP is unsuccessful in locating the transition structure for some hydrogen addition reactions, another approach is required to optimize the transition state geometry. UHF/6-311G(d,p) optimizations were able to find transition states for all six reactions. Although most UHF C−H bond lengths are fairly close to the IRCMax value, deviations from −6.0 to +9.8 pm are found (Table 4). As can be seen in Figure 4, general trends are not in agreement with the IRCMax results. QCISD/6-31G(d) performs much better, as expected. In particular, trends are in agreement (Figure 4). The low value of the bond length for the QCISD/6-31G(d) geometry is partly due to the small basis set. For the hydrogen addition to ethene, Villa et al.[33] reported a C−H bond length of 197.6 pm at the QCISD/6-311G(d,p) level. This value is closer to the IRCMax value. The correlation between the QCISD/6-31G(d) bond lengths and the

reference values would make it possible to use the QCISD/6-31G(d) values to obtain high-level bond lengths. Unfortunately, QCISD optimizations are too computationally demanding for the reactions that we want to study, even with the small 6-31G-(d) basis set. To determine a procedure that can accurately locate the transition state structure at an acceptable computational cost, we next tested the recent MPW1K method.[69] This hybrid HF-DFT model was optimized to calculate potential energy barriers and transition state geometries. Although the MPW1K method was optimized for 20 hydrogen abstraction reactions, we obtained a very good correlation for the hydrogen addition reactions. Results of the MPW1K/6-31G(d) calculations are given in Table 4. Transition states could be located for all six reactions. Although all C−H bond lengths are seriously overestimated—which is partly due to the small basis set—the correlation with the IRCMax values is striking (Figure 4): a multiple correlation coefficient of 0.9921 was obtained. The use of larger basis sets, that is, 6-31+G(d,p) and 6-311G(d,p), did decrease the difference with the reference values but did not improve the correlation. We therefore propose to use the less demanding MPW1K/6-31G(d) method in combination with the correlation between the MPW1K/6-31G(d) C−H bond length and the IRCMax value that is given in eq 7.

$$C{-}H_{IRCMax} = 0.4904 C{-}H_{MPW1K} + 94.27 \text{ pm} \qquad (7)$$

This correlation can be applied only for $C{-}H_{MPW1K}$ distances >185 pm. However, we optimized transition structures for over 40 hydrogen addition reactions, and the shortest $C{-}H_{MPW1K}$ bond length found was 190 pm.

Hydrogen Abstraction Reactions. Several groups have performed ab initio calculations for hydrogen abstraction reactions. Among the most theoretically studied reactions are the reaction of a hydrogen atom with H_2 (e.g., refs 45, 87, 88, and references cited therein) and with CH_4 (e.g., refs 36−38 and references cited therein). Sumathi et al. performed CBS-Q calculations for a large set of abstraction reactions.[42−44] Truong applied reaction class transition state theory to study hydrogen abstraction reactions,[16,17] and Blowers and Masel[41] applied different approaches to unravel the factors governing the activation energy of hydrogen abstraction reactions.

In this section, we assess the quality of B3LYP/6-311G(d,p) transition state geometries for this family of reactions. Therefore, the potential energy surfaces in the transition state region were again mapped at the CBS-QB3 level.

Two types of reactions can be distinguished. Identity hydrogen abstraction reactions, that is, $R{-}H + R^{\bullet}$, have a symmetric transition state. CBS-QB3 energies were computed for symmetric R−H−R geometries at different R−H distances. This corresponds to searching the potential energy surface in a direction orthogonal to the intrinsic reaction path at the transition state. A parabolic fit through the points around the minimum energy gave the optimal C−H distance at the transition state as well as the potential energy barrier. In Table 5 optimized and B3LYP distances are listed. The largest deviation on the CBS-QB3 potential energy barrier introduced by using the B3LYP instead of the optimized geometry is as small as +0.19 kJ/mol.

Next, the reaction paths for six nonsymmetric hydrogen abstraction reactions were investigated. The reactions were selected to cover a wide range of activation energies and transition state C−H−C distances. A similar strategy as for the radical addition reactions was followed. Table 5 lists the IRCMax and B3LYP/6-311G(d,p) optimized C−H distances and the corresponding CBS-QB3 potential energy barriers. The 6 reactions result in 12 C−H distances and 12 potential energy barriers. The largest deviation on the barriers for the B3LYP and the IRCMax geometry is −0.2 kJ/mol.

TABLE 5: Transition State Geometries for Hydrogen Abstraction Reactions from Various ab Initio Methods and Potential Energy Barriers at the CBS-QB3 Level for the Corresponding Geometries

	scan PES		B3LYP/6-311G(d,p)	
reaction	distance[a]	E_a	distance[a]	E_a
Symmetric				
$H^{\bullet} + H_2$	92.8	42.56	93.1	42.58
$CH_3^{\bullet} + CH_4$	134.0	72.58	134.7	72.65
$CH_2CH^{\bullet} + CH_2{=}CH_2$	132.4	51.82	133.4	51.97
$CH_2{=}CHCH_2^{\bullet} + CH_3CH{=}CH_2$	135.0	86.08	136.3	86.27

	IRCMax		B3LYP/6-311G(d,p)	
reaction	distance	E_a	distance	E_a
Asymmetric[b]				
$CH_3^{\bullet} + H_2$	139.2	51.39	141.8	51.20
$H^{\bullet} + CH_4$	91.0	61.47	89.0	61.28
$CH_3^{\bullet} + CH_3CH_3$	137.5	62.42	138.3	62.38
$CH_3CH_2^{\bullet} + CH_4$	132.9	77.70	132.1	77.66
$CH_3^{\bullet} + CH_3CH{=}CH_2$	145.1	45.67	147.2	45.47
$CH_2{=}CHCH_2^{\bullet} + CH_4$	128.7	124.43	126.7	124.23
$CH_3^{\bullet} + CH_2{=}CH_2$	131.5	73.39	131.6	73.39
$CH_2{=}CH^{\bullet} + CH_4$	137.0	52.62	136.8	52.62
$CH_3^{\bullet} + CH(CH_3)_3$	142.3	43.56	143.8	43.45
$(CH_3)_3C^{\bullet} + CH_4$	130.2	79.06	128.7	78.96
$CH_2{=}CH^{\bullet} + CH_3CH{=}CH_2$	149.0	27.89	150.8	27.76
$CH_2{=}CHCH_2^{\bullet} + CH_2{=}CH_2$	122.4	127.42	123.9	127.29

[a] Length (pm) of the forming C−H bond between the radical and the abstracted hydrogen atom (shown in boldface). [b] Forward and reverse reaction.

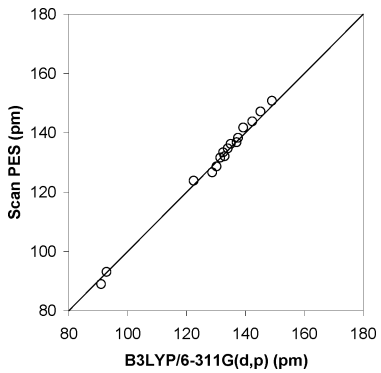

Figure 5. Bond lengths (pm) of the forming C−H bond between the radical and the abstracted hydrogen atom in the transition state of hydrogen abstraction reactions. Results from IRCMax(CBS-QB3//B3LYP/6-311G(d,p)) and from PES scanning (both indicated by scan PES in the figure) are plotted versus B3LYP/6-311G(d,p) values.

In Figure 5 the optimized and the B3LYP/6-311G(d,p) C−H bond lengths are plotted for both types of hydrogen abstraction reactions. No systematic deviation is observed. Therefore, for the hydrogen abstraction reactions, B3LYP/6-311G(d,p) geometries can be used without any correlation.

Activation Energies. Activation energies at 0 K, $\Delta E(0\text{ K})$ in eq 1, were calculated for the reactions discussed under Transition State Geometry and for two additional carbon-centered radical addition reactions. The forward and reverse activation energies were computed with CBS-QB3, applying the transition state geometry correlations given in the previous section. The systematic corrections for standard enthalpies of formation, proposed under Standard Enthalpy of Formation for Stable Molecules, were not used here. Indeed, the number of atoms does not change in going from the reactants to the transition state, and the systematic corrections do not have any

TABLE 6: Calculated and Experimental Activation Energies (kJ/mol) at 0 K, ΔE(0 K), for Three Families of Radical Reactions from Various Levels of Theory

		CBS-QB3[b]		B3LYP/6-31G(d)		B3LYP/6-311G(d,p)		exptl[a]	
	reaction	ΔE_{for}(0 K)	ΔE_{rev}(0 K)	ΔE_{for}(0 K)	ΔE_{rev}(0 K)	ΔE_{for}(0 K)	ΔE_{rev}(0 K)	ΔE_{for}(0 K)	ΔE_{rev}(0 K)
					Radical Addition/β-Scission				
1	$CH_3^{\bullet} + CH_2{=}CH_2$	31.1	122.7	27.7	126.2	31.9	117.6	28.1/30.8/30.4[c]	123.7/135.9/123.7[c]
2	$CH_3CH_2^{\bullet} + CH_2{=}CH_2$	27.3	116.3	29.2	115.3	34.4	108.3	26.6/30.0	113.7/117.4/118.1
3	$CH_3CH_2CH_2^{\bullet} + CH_2{=}CH_2$	26.4	117.8	28.3	118.0	34.5	109.5	24.1/29.6	
4	$(CH_3)_2CH^{\bullet} + CH_2{=}CH_2$	21.6	107.3	30.8	104.3	36.1	96.2	27.9	
5	$(CH_3)_3C^{\bullet} + CH_2{=}CH_2$	14.7	96.7	32.7	89.1	37.2	81.4	28.5	
6	$CH_2{=}CHCH_2^{\bullet} + CH_2{=}CH_2$	52.6	82.3	55.1	80.5	61.7	74.6		93.4
7	$CH{\equiv}CCH_2^{\bullet} + CH_2{=}CH_2$	43.1	87.3	46.8	81.1	52.2	76.5		
8	$CH_2CH^{\bullet} + CH_2{=}CH_2$	13.7	149.5	12.8	153.5	17.6	144.1		
9	$CH_3^{\bullet} + CH{\equiv}CH$	36.9	139.9	34.6	153.2	36.3	139.2		134.5/175.3
10	$CH_3^{\bullet} + CH_3CH{=}CH_2$	35.2	122.9	38.1	123.6	42.4	115.3	33.0/29.0[c]	106.7/122.0/133.5/121.2[c]
11	$CH_3^{\bullet} + CH_2{=}CHCH{=}CH_2$	17.1	156.9	17.0	158.2	20.3	151.1		155.4
1	$H^{\bullet} + CH_2{=}CH_2$	10.1	154.8	1.7	163.7	3.4	159.2	9.1	
2	$H^{\bullet} + CH{\equiv}CH$	16.4	162.8	11.0	177.9	8.4	168.1	10.5	
3	$H^{\bullet} + CH_3CH{=}CH_2$	15.4	147.4	7.8	150.6	9.0	148.4	14.3	
4	$H^{\bullet} + CH_2{=}CHCH{=}CH_2$	2.8	194.6	0.0	207.2	0.0	200.9		
5	$H^{\bullet} + CH_2{=}C{=}CH_2$	18.9	253.5	14.7	255.0	15.3	251.0	8.4/10.9	
6	$H^{\bullet} + CH_2{=}C(CH_3)_2$	4.6	149.5	0.0	162.8	0.0	157.8	2.6/6.5	
					H Abstraction				
1	$H^{\bullet} + H_2$	39.8		17.2		15.0		16.7/33.7	
2	$CH_3^{\bullet} + CH_4$	71.0		59.2		60.7		55.4/60.7/61.9[d]	
3	$CH_2CH^{\bullet} + CH_2{=}CH_2$	44.5		39.0		41.0			
4	$CH_2{=}CHCH_2^{\bullet} + CH_3CH{=}CH_2$	79.3		78.1		79.6			
5	$CH_3^{\bullet} + H_2$	56.0	58.8	39.6	38.7	41.6	35.4	40.6/56.7/64.8/45.2[d]	37.0/51.9/68.3/45.6[d]
6	$CH_3^{\bullet} + CH_3CH_3$	58.9	75.2	48.6	69.0	50.5	70.9	47.0/55.1/50.6[d]	
7	$CH_3^{\bullet} + CH_3CH{=}CH_2$	42.9	117.7	33.9	116.0	36.0	116.2	32.3/35.5	91.0
8	$CH_3^{\bullet} + CH_2{=}CH_2$	69.3	47.2	58.7	40.2	61.2	41.6	45.2/61.6/70.1	24.2
9	$CH_3^{\bullet} + CH(CH_3)_3$	38.3	73.9	33.8	84.5	35.1	83.7	31.0/44.9/51.2	
10	$CH_2{=}CH^{\bullet} + CH_3CH{=}CH_2$	21.2	118.2	16.5	117.0	18.6	118.4	17.6/22.6	

[a] Derived from experimental Arrhenius activation energies[90] using unscaled B3LYP/6-311G(d,p) thermochemistry. [b] Using the optimized transition state geometries as described in the text. [c] Reference 30. [d] Reference 19.

influence on the calculated activation energies. For comparison, B3LYP/6-31G(d) and B3LYP/6-311G(d,p) activation energies were computed as well. Unscaled zero-point energies were used in the B3LYP DFT calculations. Use of a scaling factor of 0.9806[89] changes the activation energies in a systematic way by <0.5 kJ/mol. Table 6 lists the results as well as experimental data where available. The experimental values were obtained from the NIST Chemical Kinetics Database[90] and from additional literature data.[19,30] The experimental Arrhenius activation energies from the NIST database were converted to ΔE(0 K) by using the thermochemistry from the B3LYP/6-311G(d,p) calculations in eq 8,[59] in which $E_{a,Arrhenius}(T)$ is the experimental

$$E_{a,Arrhenius}(T) = \Delta H^{\ddagger}(T) + (1 - \Delta n^{\ddagger})RT = \Delta E(0\text{ K}) + \Delta E_{vib,trans,rot}(0 \rightarrow T) + (1 - \Delta n^{\ddagger})RT \quad (8)$$

Arrhenius activation energy at temperature T, $\Delta n^{\ddagger}$ is the change in the number of molecules in going from the reactants to the transition state, and $\Delta E_{vib,trans,rot}(0 \rightarrow T)$ is the change in internal energy due to translation, vibrational motion, and rotational motion. The harmonic oscillator approximation was used here; that is, internal rotations were not treated separately. In a previous publication[71] it was shown that internal rotations have only a minor influence on the calculated activation energies. They are however important to obtain accurate pre-exponential factors. The large variation in the experimental values makes a thorough comparison with the theoretical predictions difficult. Moreover, for hydrogen radical addition reactions and hydrogen abstraction reactions, tunneling is an important effect at temperatures at which the experimental data were obtained. This effect lowers the apparent activation energy. In the following we will therefore focus on the theoretical values and discuss their behavior.

Influence of Basis Set Size on Predicted Activation Energies for DFT Methods. Under Standard Enthalpy of Formation for Stable Molecules, a significant influence of the basis set size on the calculated standard enthalpies of formation in B3LYP DFT was observed. Here, we want to investigate if the same is true for activation energies. Activation energies from B3LYP/6-31G(d) and B3LYP/6-311G(d,p) calculations are given in Table 6. For the carbon-centered radical addition reactions, the activation energies increase by ~4 kJ/mol when the basis set is enlarged. A similar effect is seen for hydrogen addition reactions, although the effect is smaller. All activation energies for the reverse β-scission reactions decrease by on average 8 kJ/mol when the basis set is enlarged. An important fraction of these effects is caused by a change in the basis set superposition error[80] (BSSE) for the forming bond. The large BSSE for the 6-31G(d) basis artificially lowers the electronic energy of the transition state relative to the energy of the reactants and lowers the product energy even more. Enlarging the basis set size decreases the BSSE and thus shifts up the relative energies, thereby increasing the radical addition barrier and decreasing the β-scission barrier. For the methyl radical addition to ethene using the 6-31G(d) basis set counterpoise BSSEs[80] of 7.1 and 13.7 kJ/mol are calculated for the transition state and for the product, respectively. For the larger 6-311G(d,p) basis set lower BSSEs are computed, that is, 3.6 and 6.9 kJ/mol. Although the basis set size has an influence on the computed activation energies, the change in barrier height with basis set size is highly systematic and does not influence the relative reactivity.

For the hydrogen abstraction reactions, the barrier usually increases with the size of the basis set. The increments are smaller and less systematic than for the radical addition reactions. During the hydrogen abstraction reaction one C−H

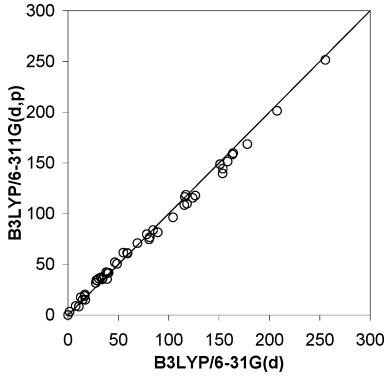

Figure 6. Influence of the basis set size on the activation energy (kJ/mol) of hydrogen abstraction and radical addition reactions in B3LYP DFT calculations.

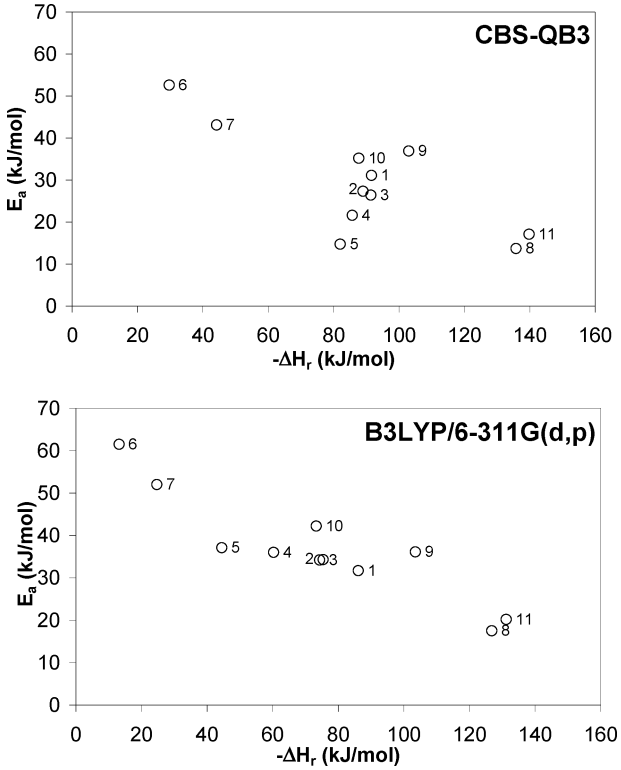

Figure 7. Activation energies of carbon-centered radical addition reactions versus the standard reaction enthalpy. The reactions are labeled according to the numbering in Table 6.

bond is broken and another is formed. This mechanism masks the effect of the BSSE.

In Figure 6 both of the DFT activation energies are plotted. As can be concluded from this parapraph, the effect of basis set size on the computed B3LYP DFT activation energy is rather small and highly systematic for the reactions discussed in this paper. In the following, we will therefore compare the CBS-QB3 results only with the B3LYP/6-311G(d,p) values.

CBS-QB3 and B3LYP DFT Activation Energies. Unfortunately, the discrepancies between the various experimental activation energies are too large to quantitatively assess the accuracy of the CBS-QB3 results, as we did under Standard Enthalpy of Formation for Stable Molecules. In view of the highly accurate reproduction of the standard enthalpies of formation, we expect the CBS-QB3 activation energies to have similar quantitative accuracy.

In Figure 7a the CBS-QB3 activation energies for the carbon-centered radical addition reactions are plotted versus the reaction

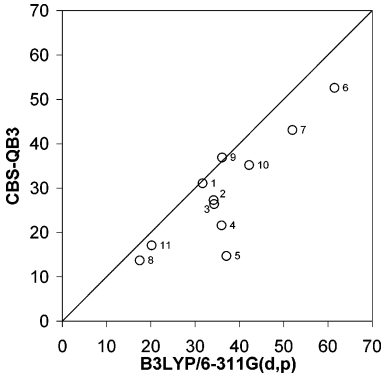

Figure 8. CBS-QB3 activation energies (kJ/mol) versus B3LYP/6-311G(d,p) activation energies for carbon-centered radical addition reactions. The reactions are labeled according to the numbering in Table 6.

enthalpy. The main trend follows an Evans−Polanyi relation; that is, the activation energy is lower for more exothermic reactions. However, the addition of methyl, ethyl, isopropyl, and ter-isobutyl radicals to ethene does not follow this trend (see reactions 1−5 in Table 6 and Figure 7). For these reactions, the CBS-QB3 activation energy is higher for the more exothermic reactions. The low activation energy for ter-isobutyl radical additions has been reported previously[22,29] on the basis of high-level ab initio calculations. It is believed to be caused by polar effects, which lead to a relatively strong nucleophilic character of the ter-isobutyl radical, which stabilizes the transition state.[30] Indeed, a Mulliken population analysis for the transition states at the UHF level shows that the charge transfer from the radical to the olefin increases in the same order as the activation energy decreases. Summarizing, from the CBS-QB3 results we find that the reactivity of the addition reactions studied is governed by a combination of enthalpic and polar factors. This is in agreement with the conclusions from a recent review by Fisher and Radom.[30]

In contrast to the behavior observed in the CBS-QB3 results, the B3LYP DFT activation energies are mainly determined by the reaction enthalpy, and polar effects are found to be of minor importance (Figure 7b). The B3LYP activation energies for the addition reaction actually increase in the following order: methyl, ethyl, 1-propyl, isopropyl to ter-isobutyl radical addition to ethene. The B3LYP DFT calculations seem to neglect the polar effect. This deficiency might be related to the problems observed in reproducing correct ionization energies (IE). None of the current exchange correlation potentials succeed in accurately reproducing the experimental IE of the hydrogen atom. Rather, errors of >5 eV are found.[66] This is believed to be related to deficiencies in the long-range behavior of the exchange correlation potentials generated by current functionals.[66] Because the magnitude of the nucleophilic effect is related to the difference between the IE of the radical and the electron affinity of the alkene,[30] we believe these deficiencies are at the origin of the observed behavior of the B3LYP DFT barriers.

To illustrate the previous discussion, B3LYP activation energies were plotted versus CBS-QB3 values in Figure 8. Except for the isopropyl and the ter-isobutyl radical addition reactions (labeled 4 and 5), where nucleophilic effects are important, a rather good correlation is observed, with a tendency of the B3LYP DFT method to overestimate the radical addition barrier. A rather good correlation is also observed for the reverse β-scission barrier (Table 6), although deviations of up to 15 kJ/mol can still be seen when nucleophilic effects are important.

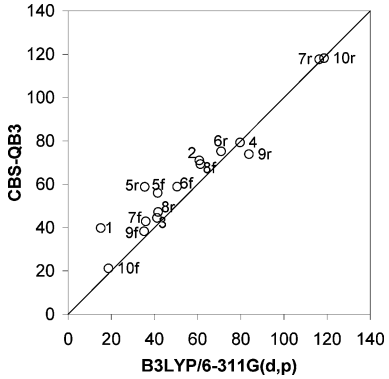

Figure 9. CBS-QB3 versus B3LYP/6-311G(d,p) activation energies (kJ/mol) for hydrogen abstraction reactions. The reactions are labeled according to the numbering in Table 6; "f" indicates forward and "r" reverse reactions.

For the addition of hydrogen radicals to alkenes, B3LYP strongly underestimates the low addition activation energies (Table 6). For the activation energies of the reverse β-scission reactions, on the other hand, the agreement between B3LYP and CBS-QB3 activation energies is rather good. However, the activation energies for hydrogen addition are so low that the large barriers for the reverse β-scission reactions are almost entirely dominated by the reaction enthalpy. Note, however, that the β-scission activation energy for reaction 6 deviates by 8.3 kJ/mol from the CBS-QB3 value.

For hydrogen abstraction reactions, B3LYP DFT is capable of reproducing the main trends in the CBS-QB3 activation energies (Table 6 and Figure 9) but fails to reproduce important details. In particular, for reactions in which a hydrogen radical is involved (reactions 1 and reverse 5), deviations of up to 25 kJ/mol are found. This has been related to the presence of self-interaction in the B3LYP functional.[87,88] For the other reactions studied, deviations ranging from -10 to $+10$ kJ/mol are observed.

Conclusions

The present paper discusses the accuracy of post-HF CBS-QB3 and B3LYP density functional calculations for hydrocarbon thermochemistry and radical reactivity. It is found that standard enthalpies of formation of hydrocarbon molecules and radicals are accurately determined by the CBS-QB3 method, provided a systematic correction per carbon atom and per hydrogen atom is taken into account. This is in contrast to B3LYP density functional theory, where significant deviations are found, in particular for larger hydrocarbons.

B3LYP density functional theory allows the geometry of transition states for hydrogen abstraction reactions to be described with a precision similar to that of computationally much more expensive methods. Radical addition reactions, however, are strongly exothermic and characterized by rather early transition states. B3LYP DFT has the tendency to overestimate the length of the forming bond for this family of reactions as compared to high-level IRCMax results and, therefore, locates the transition state too early on the potential energy surface. Agreement with high-level transition state geometries for radical addition reactions can still be obtained from DFT calculations using the appropriate exchange correlation functional, in combination with the linear correlations (eqs 6 and 7) proposed in this paper.

It is clearly demonstrated that the reactivity of carbon-centered radical addition reactions to alkenes is governed by a combination of polar and enthalpic factors. In particular, polar effects are better accounted for by the CBS-QB3 method than by B3LYP density functional theory. Although better agreement between the DFT and CBS-QB3 activation energies is found for hydrogen abstraction reactions, deviations still range from -10 to $+10$ kJ/mol.

Acknowledgment. We thank Peter Vansteenkiste for performing part of the calculations reported in this paper. M.S. is grateful to the Fund for Scientific Research-Flanders, Belgium (F.W.O.-Vlaanderen) for a Research Assistantship.

References and Notes

(1) Clymans, P. J.; Froment, G. F. *Comput. Chem. Eng.* **1984**, *8*, 137.
(2) Susnow, R. G.; Dean, A. M.; Green, W. H.; Peczak, P.; Broadbelt, L. J. *J. Phys. Chem. A* **1997**, *101*, 3731.
(3) De Witt, M. J.; Dooling, D. J.; Broadbelt, L. J. *Ind. Eng. Chem. Res.* **2000**, *39*, 2228.
(4) Green, W. H.; Barton, P. I.; Bhattacharjee, B.; Matheu, D. M.; Schwer, D. A.; Song, J.; Sumathi, R.; Carstensen, H.-H.; Dean, A. M.; Grenda, J. M. *Ind. Eng. Chem. Res.* **2001**, *40*, 5370.
(5) Wauters, S.; Marin, G. B. *Ind. Eng. Chem. Res.* **2002**, *41*, 2379.
(6) Pilling, M. J. *Annu. Rev. Phys. Chem.* **1996**, *47*, 81.
(7) Ma, X.; Schobert, H. H. *J. Phys. Chem. A* **2000**, *104*, 1064.
(8) Ma, X.; Schobert, H. H. *Ind. Eng. Chem. Res.* **2001**, *40*, 743.
(9) Barone, V.; Orlandini, L. *Chem. Phys. Lett.* **1995**, *246*, 45.
(10) Bottoni, A. *J. Chem. Soc., Perkin Trans. 2* **1996**, 2041.
(11) Korth, H.-G.; Sicking, W. *J. Chem. Soc., Perkin Trans. 2* **1997**, 715.
(12) Jursic, B. S. *J. Chem. Soc., Perkin Trans. 2* **1997**, 637.
(13) Xiao, Y.; Longo, J. M.; Hieshima, G. B.; Hill, R. J. *Ind. Eng. Chem. Res.* **1997**, *36*, 4033.
(14) Arnaud, R.; Bugaud, N.; Vetere, V.; Barone, V. *J. Am. Chem. Soc.* **1998**, *120*, 5733.
(15) Susnow, R. G.; Dean, A. M.; Green, W. H. *Chem. Phys. Lett.* **1999**, *312*, 262.
(16) Truong, T. N.; Truong, T.-T. T. *Chem. Phys. Lett.* **1999**, *314*, 529.
(17) Truong, T. N. *J. Chem. Phys.* **2000**, *113*, 4957.
(18) Lynch, B. J.; Truhlar, D. G. *J. Phys. Chem. A* **2001**, *105*, 2936.
(19) Kang, J. K.; Musgrave, C. B. *J. Chem. Phys.* **2001**, *115*, 11040.
(20) Wong, M. W.; Pross, A.; Radom, L. *J. Am. Chem. Soc.* **1993**, *115*, 11050.
(21) Wong, M. W.; Pross, A.; Radom, L. *J. Am. Chem. Soc.* **1994**, *116*, 6284.
(22) Wong, M. W.; Pross, A.; Radom, L. *J. Am. Chem. Soc.* **1994**, *116*, 11938.
(23) Wong, M. W.; Radom, L. *J. Phys. Chem.* **1995**, *99*, 8582.
(24) Wong, M. W.; Radom, L. *J. Phys. Chem. A* **1998**, *102*, 2237.
(25) Smith, B. J.; Radom, L. *J. Phys. Chem. A* **1998**, *102*, 10787.
(26) Mayer, P. M.; Parkinson, C. J.; Smith, D. M.; Radom, L. *J. Chem. Phys.* **1998**, *108*, 604.
(27) Parkinson, C. J.; Mayer, P. M.; Radom, L. *J. Chem. Soc., Perkin Trans. 2* **1999**, *11*, 2305.
(28) Henry, D. J.; Parkinson, C. J.; Mayer, P. M.; Radom, L. *J. Phys. Chem. A* **2001**, *105*, 6750.
(29) Heuts, J. P. A.; Hilbert, R. G.; Radom, L. *J. Phys. Chem.* **1996**, *100*, 18997.
(30) Fischer, H.; Radom, L. *Angew. Chem., Int. Ed.* **2001**, *40*, 1340.
(31) Hase, W. L.; Schlegel, H. B.; Balbyshed, V.; Page, M. *J. Phys. Chem.* **1996**, *100*, 5354.
(32) Villà, J.; González-Lafont, A.; Lluch, J. M.; Truhlar, D. G. *J. Am. Chem. Soc.* **1998**, *120*, 5559.
(33) Villà, J.; Corchado, J. C.; González-Lafont, A.; Lluch, J. M.; Truhlar, D. G. *J. Phys. Chem. A* **1999**, *103*, 5061.
(34) Zhang, X.; Ding, Y.; Li, Z.; Huang, X.; Sun, C. *J. Phys. Chem. A* **2000**, *104*, 8375.
(35) Miller, J. A.; Klippenstein, S. J.; Robertson, S. H. *J. Phys. Chem. A* **2000**, *104*, 7525.
(36) Espinosa-Garcia, J.; Corchado, J. C. *J. Phys. Chem.* **1996**, *100*, 1651.
(37) Espinosa-Garcia, J. *J. Chem. Phys.* **2002**, *116*, 10664.
(38) Pu, J. Z.; Truhlar, D. G. *J. Chem. Phys.* **2002**, *116*, 1468.
(39) Viskolcz, B.; Lendvay, G.; Seres, L. *J. Phys. Chem. A* **1997**, *101*, 7119.
(40) Marsi, I.; Viskolcz, B.; Seres, L. *J. Phys. Chem. A* **2000**, *104*, 4497.
(41) Blowers, P.; Masel, R. *AIChE J.* **2000**, *46*, 2041.
(42) Sumathi, R.; Carstensen, H.-H.; Green, W. H., Jr. *J. Phys. Chem. A* **2001**, *105*, 6910.
(43) Sumathi, R.; Carstensen, H.-H.; Green, W. H., Jr. *J. Phys. Chem. A* **2001**, *105*, 8969.

(44) Sumathi, R.; Carstensen, H.-H.; Green, W. H., Jr. *J. Phys. Chem. A* **2002**, *106*, 5474.
(45) Mielke, S. L.; Garrett, B. C.; Peterson, K. A. *J. Chem. Phys.* **2002**, *116*, 4142.
(46) Byrd, E. F. C.; Sherrill, C. D.; Head-Gordon, M. *J. Phys. Chem. A* **2001**, *105*, 9736.
(47) Li, Z.; Rogers, D. W.; McLafferty, F. J.; Mandziuk, M.; Podosenin, A. V. *J. Phys. Chem. A* **1999**, *103*, 426.
(48) Chuang, Y.-Y.; Coitiño, E. L.; Truhlar, D. G. *J. Phys. Chem. A* **2000**, *104*, 446.
(49) Feller, D.; Peterson, K. A. *J. Chem. Phys.* **1999**, *110*, 8384.
(50) Feller, D.; Dixon, D. A. *J. Phys. Chem. A* **2000**, *104*, 3048.
(51) Parthiban, S.; Martin, J. M. L.; Liebman, J. F. *Mol. Phys.* **2002**, *100*, 453.
(52) Becke, A. D. *J. Chem. Phys.* **1993**, *98*, 5648.
(53) Stephens, P. J.; Devlin, F. J.; Chabalowski, C. F.; Frisch, M. J. *J. Phys. Chem.* **1994**, *98*, 11623.
(54) Nyden, M. R.; Petersson, G. A. *J. Chem. Phys.* **1981**, *75*, 1843.
(55) Ochterski, J. W.; Petersson, G. A.; Montgomery, J. A., Jr. *J. Chem. Phys.* **1999**, *104*, 2598.
(56) Montgomery, J. A., Jr.; Frisch, M. J.; Ochterski, J. W.; Petersson, G. A. *J. Chem. Phys.* **1999**, *110*, 2822.
(57) Montgomery, J. A., Jr.; Frisch, M. J.; Ochterski, J. W.; Petersson, G. A. *J. Chem. Phys.* **2000**, *112*, 6532.
(58) Hehre, W. J.; Radom, L.; von Ragué Schleyer, P.; Pople, J. A. *Ab Initio Molecular Orbital Theory*; Wiley: New York, 1986.
(59) Jensen, F. *Introduction to Computational Chemistry*; Wiley: New York, 1999.
(60) Chen, W.; Schlegel, H. B. *J. Chem. Phys.* **1994**, *101*, 5957.
(61) Curtiss, L. A.; Raghavachari, K.; Trucks, G. W.; Pople, J. A. *J. Chem. Phys.* **1991**, *94*, 7221.
(62) Curtiss, L. A.; Raghavachari, K.; Redfern, P. C.; Rassolov, V.; Pople, J. A. *J. Chem. Phys.* **1998**, *109*, 7764.
(63) Curtiss, L. A.; Redfern, P. C.; Raghavachari, K.; Pople, J. A. *J. Chem. Phys.* **2001**, *114*, 108.
(64) Curtiss, L. A.; Raghavachari, K.; Redfern, P. C.; Pople, J. A. *J. Chem. Phys.* **1997**, *106*, 1063.
(65) Martin, J. M. L.; de Oliveira, G. *J. Chem. Phys.* **1999**, *111*, 1843.
(66) Koch, W.; Holthausen, M. C. *A Chemist's Guide to Density Functional Theory*, 2nd ed.; Wiley-VCH: Weinheim, Germany, 2001.
(67) Frisch, M. J.; Trucks, G. W.; Schlegel, H. B.; Scuseria, G. E.; Robb, M. A.; Cheeseman, J. R.; Zakrzewski, V. G.; Montgomery, J. A., Jr.; Stratmann, R. E.; Burant, J. C.; Dapprich, S.; Millam, J. M.; Daniels, A. D.; Kudin, K. N.; Strain, M. C.; Farkas, O.; Tomasi, J.; Barone, V.; Cossi, M.; Cammi, R.; Mennucci, B.; Pomelli, C.; Adamo, C.; Clifford, S.; Ochterski, J.; Petersson, G. A.; Ayala, P. Y.; Cui, Q.; Morokuma, K.; Malick, D. K.; Rabuck, A. D.; Raghavachari, K.; Foresman, J. B.; Cioslowski, J.; Ortiz, J. V.; Baboul, A. G.; Stefanov, B. B.; Liu, G.; Liashenko, A.; Piskorz, P.; Komaromi, I.; Gomperts, R.; Martin, R. L.; Fox, D. J.; Keith, T.; Al-Laham, M. A.; Peng, C. Y.; Nanayakkara, A.; Gonzalez, C.; Challacombe, M.; Gill, P. M. W.; Johnson, B.; Chen, W.; Wong, M. W.; Andres, J. L.; Gonzalez, C.; Head-Gordon, M.; Replogle, E. S.; Pople, J. A. *Gaussian 98*, rev A.7; Gaussian, Inc.: Pittsburgh, PA, 1998.
(68) Malick, D. K.; Petersson, G. A.; Montgomery, J. A., Jr. *J. Chem. Phys.* **1998**, *108*, 5704.
(69) Lynch, B. J.; Fast, P. L.; Harris, M.; Truhlar, D. G. *J. Phys. Chem. A* **2000**, *104*, 4811.
(70) Laidler, K. J. *Chemical Kinetics*; Harper Collins Publishers: New York, 1987.
(71) Van Speybroeck, V.; Van Neck, D.; Waroquier, M.; Wauters, S.; Saeys, M.; Marin, G. B. *J. Phys. Chem. A* **2000**, *104*, 10939.
(72) Irikura, K. K. In *Computational Thermochemistry: Prediction and Estimation of Molecular Thermodynamics*; ACS Symposium Series 677; Irikura, K. K.; Frurip, D. J., Eds.; American Chemical Society: Washington, DC, 1998.
(73) Cioslowski, J.; Schimeczek, M.; Liu, G.; Stoyanov, V. *J. Chem. Phys.* **2000**, *113*, 9377.
(74) Afeefy, H. Y.; Liebman, J. F.; Stein, S. E. *Neutral Thermochemical Data* in *NIST Chemistry WebBook, NIST Standard Reference Database Number 69*; Linstrom, P. J., Mallard, W. G., Eds.; National Institute of Standards and Technology: Gaithersburg, MD, 2001; http://webbook.nist.gov.
(75) Curtiss, L. A.; Raghavachari, K.; Redfern, P. C.; Pople, J. A. *J. Chem. Phys.* **2000**, *112*, 7374.
(76) Tsang, W. In *Energetics of Organic Free Radicals*; Martinho Simoes, J. A., Greenberg, A., Liebman, J. F., Eds.; Blackie Academic and Professional: London, U.K., 1996.
(77) Chase, M. W., Jr. *J. Phys. Chem. Ref. Data* **1998**, *9*, 1.
(78) Cohen, N.; Benson, S. W. In *The Chemistry of Alkanes and Cycloalkanes*; Patai, Rappoport, Eds.; Wiley: New York: 1992.
(79) Pedley, J. B. *Thermochemical Data and Structures of Organic Compounds*; Thermodynamics Research Center: College Station, TX, 1994; Vol. 1.
(80) van Duijneveldt, F. B.; van Duijneveldt-van de Rijdt, J. G. C. M.; van Lenthe, J. H. *Chem. Rev.* **1994**, *94*, 1873.
(81) Baerends, E. J.; Branchadell, V.; Sodupe, M. *Chem. Phys. Lett.* **1997**, *265*, 481.
(82) Redfern, P. C.; Zapol, P.; Curtiss, L. A.; Raghavachari, K. *J. Phys. Chem. A* **2000**, *104*, 5850.
(83) Kedziora, G. S.; Pople, J. A.; Rassolov, V. A.; Ratner, M. A.; Redfern, P. C.; Curtiss, L. A. *J. Chem. Phys.* **1999**, *110*, 7123.
(84) Roth, W. R.; Adamczak, O.; Breukmann, R.; Lennartz, H.-W.; Boese, R. *Chem. Ber.* **1991**, *124*, 2499.
(85) Curtiss, L. A.; Raghavachari, K.; Redfern, P. C.; Pople, J. A. *J. Chem. Phys.* **2000**, *112*, 1125.
(86) Solling, T. I.; Smith, D. M.; Radom, L.; Freitag, M. A.; Gordon, M. S. *J. Chem. Phys.* **2001**, *115*, 8758.
(87) Patchkovskii, S.; Ziegler, T. *J. Chem. Phys.* **2002**, *116*, 7806.
(88) Johnson, B. G.; Gonzales, C. A.; Gill, P. M. W.; Pople, J. A. *Chem. Phys. Lett.* **1994**, *221*, 100.
(89) Scott, A. P.; Radom, L. *J. Phys. Chem.* **1996**, *100*, 16502.
(90) NIST. *Chemical Kinetics Database on the Web*, public beta release 1.1; Standard Reference Database 17, version 7.0 (Web version), 2000; http://kinetics.nist.gov.